A Charged Contour Model for Cardiac SPECT Segmentation

Ronghua Yang[a], Majid Mirmehdi[a], David Hall[b*]

[a]Department of Computer Science, University of Bristol, Bristol BS8 1UB, UK,
[b]Department of Medical Physics and Bioengineering, Bristol General Hospital, Guinea Street, Bristol, BS1 6SY, UK

Abstract. This paper presents a new deformable model for object detection, based on charged particle dynamics and geometric contour propagation, applied to the segmentation of the left ventricle of the heart in SPECT images. The model detects object boundaries with a charged active contour that propagates under the influence of Lorentz forces in an image-based electrostatic field. We find positions of vector field divergence for automatic initialisation of the contour. Experimental results on a dataset of 160 images are evaluated against hand-labelled groundtruth data.

1 Introduction

Myocardial perfusion scintigraphy (MPS) is carried out routinely in hospitals around the world, with the most common form of image acquisition being Single Photon Emission Computed Tomography (SPECT). Cardiac SPECT images provide information on myocardial viability, perfusion, and function, and this helps determine the presence, location, extent and severity of coronary heart disease. The functional parameters that assist the diagnosis include cardiac end-diastolic and end-systolic volumes and left ventricular ejection fraction which are calculated by detecting myocardial borders of the left ventricle (LV).

Active contour models have played a vital role in medical image analysis ever since the parametric snake model was introduced [5]. They have been used in cardiac SPECT segmentation with various modifications, e.g. see [2, 6]. However, they still suffer from problems such as edge leakage and high sensitivity to contour initialization.

In this work we propose a novel active contour model for LV segmentation in cardiac SPECT, namely the charged contour model (CCM). This is motivated by the recently introduced charged particle model (CPM) [4]. CCM defines a geometric active contour based on charged particle dynamics. The charged contour deforms under the influence of Lorentz forces in an image-based electrostatic field, and provides accurate boundary information. We also propose an automatic initialisation approach based on vector divergence estimation, which helps towards the automatic detection of both interior and exterior boundaries simultaneously.

In Section 2, we introduce the basis of our proposed model, charged particle dynamics, along with the CPM model [4] and its drawbacks. The structure of CCM is then outlined in Section 3, followed by the automatic initialisation procedure in Section 4. Experimental results are presented in Section 5, and the last section concludes the paper.

2 Charged Particle Dynamics and CPM

In charged particle dynamics, a set of positively charged, freely moving particles is placed in a field that has a distribution of negative fixed charges, forming an electrostatic field. Each charged particle is then attracted towards the fixed charges under the influence of a mesh-to-particle (Lorentz) force. At the same time, all positive free charges are repelled by one another by the repulsive particle-to-particle (Coulomb) force.

Consider an electrostatic field with M negative fixed charges and N positive free particles, with the kth fixed charge at grid position $\mathbf{R}_k$ with charge $e_k < 0$, and the ith free particle at position $\mathbf{r}_i$ with charge $q_i > 0$. Then, the Lorentz force $\mathbf{F}_l$ (in the absence of a magnetic field) and Coulomb force $\mathbf{F}_c$ acting on the ith free particle are defined as [4]:

$$\mathbf{F}_l(\mathbf{r}_i) = q_i \sum_{k=1,\mathbf{R}_k \neq \mathbf{r}_i}^{M} \frac{e_k}{4\pi\epsilon_0} \frac{\mathbf{r}_i - \mathbf{R}_k}{|\mathbf{r}_i - \mathbf{R}_k|^3} \quad \text{and} \quad \mathbf{F}_c(\mathbf{r}_i) = q_i \sum_{j=1,j\neq i}^{N} \frac{q_j}{4\pi\epsilon_0} \frac{\mathbf{r}_i - \mathbf{r}_j}{|\mathbf{r}_i - \mathbf{r}_j|^3}, \tag{1}$$

where ϵ_0 is the electric permittivity of free space. These equations state that the Lorentz force $\mathbf{F}_l$ acting on each free particle is the sum of the forces imposed onto it by all the fixed charges in the electrostatic field, and that the Coulomb force $\mathbf{F}_c$ is the sum of the forces imposed onto the particle by all the other free particles and as this changes dynamically with distance between particles, it needs to be updated over each particle movement. These two forces can

---

*Email: ronghua@cs.bris.ac.uk, majid@cs.bris.ac.uk, david.hall@ubht.nhs.uk
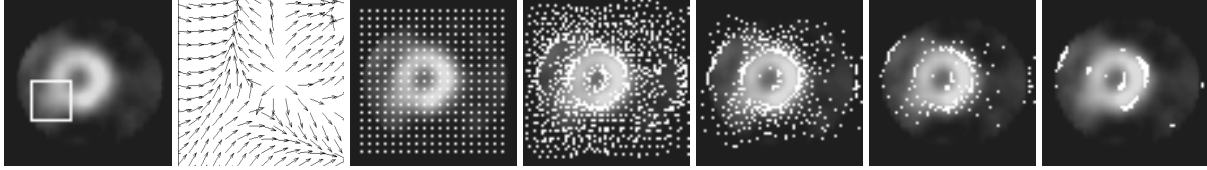
Figure 1. From left: original 64×64 cardiac SPECT image of a LV with a window highlighting a weak edge area, the normalized Lorentz force field within the windowed area, the initialized CPM [4] particles, and iterations of particle movements with the final result on the right.

play the roles of external and internal forces respectively in a deformable model for image segmentation. In CPM [4], the total force on each particle is a weighted sum of normalized Lorentz and Coulomb forces, reduced by a damping factor dominated by the particle speed at the previous step. As the weight of the Lorentz force is always larger than that of the Coulomb force, particles are primarily attracted towards object boundaries by Lorentz forces while Coulomb forces advance the particles along the boundaries. Thus, the boundaries can be recovered given proper dynamic particle addition and deletion during particle movements.

The CPM model [4] benefits from initialisation that is largely insensitive to placement. Nevertheless, it is very computationally intensive as (a) particles have to advance along the boundaries until they are evenly distributed (around the boundaries), and (b) particles are added and deleted dynamically at each iteration. Although a damping factor is used to reverse the direction of acceleration when a particle crosses an edge, the particle will still move as long as its speed is not exactly zero, and therefore oscillations occur at the boundaries and particle convergence needs to be detected by some criterion. Above all, CPM can not guarantee closed contours, which inevitably results in gaps in the recovered object boundaries particularly if the object is occluded or has weak edges, as shown in the example of a 64×64 cardiac SPECT image in Fig.1 (larger versions of all images in the paper can be viewed online[1]). The highly diffused edge area (see square on the original image) is significantly influenced by the stronger edges nearby, hence its Lorentz forces, especially those on the edge center, show tendency towards those stronger edges. As the Lorentz forces always dominate the direction of particle movements, particles which have arrived at the weak edges will continue moving to the stronger edges with the weak edge left unmarked. CPM therefore can not successfully deal with the SPECT images in our application as shown in Fig.1.

3   Proposed Charged Contour Model (CCM)

We propose a model built on the basis of charged particle dynamics combined with active contour evolution. This model detects objects starting with a positively charged active contour that propagates in an image-based electrostatic field, distributed with negative fixed charges, under the influence of Lorentz forces. The Coulomb force becomes redundant in our CCM model as repelling particle forces are no longer necessary. Instead, we use geometric curvature flow for model regulation, implemented using a level-set representation. CCM performs better than CPM in terms of (a) faster convergence, (b) steady equilibrium state, (c) less sensitivity in highly-textured images and (d) providing boundaries that are continuous closed contours.

A positively charged contour is placed in an image-based electrostatic field in which the fixed charge at every pixel position is computed as $e_k = -f(x_k, y_k) \leq 0$, for $k = 1, .., M$, where $f(x, y)$ is the image edge map and M is now the size of the image. Then, the Lorentz force field is obtained using the equation for $\mathbf{F}_l$ in (1). As the Lorentz force decays with squared distance, it produces weak flows in homogeneous areas and stronger flows closer to edges. This is an undesirable feature since, driven by these forces, the active contour can hardly move in homogeneous areas, whilst moving fast in edge areas where it is likely to oscillate around edges. As a result, we perform a weighted normalisation of the Lorentz force field to speed up the model convergence, such that the normalised field has strong flows in homogeneous areas and weak, or close to zero, flows near edges which finally stop the contour. At edge locations the strength of the flows are already drastically reduced due to the counteractions among the surrounding fixed charges. This is a good indication of where the real edges are located. Therefore, our edge-preserving weighted normalisation process is built on the information supplied by the edge map:

$$\mathbf{F}'_l(\mathbf{r}_k) = \frac{\mathbf{F}_l(\mathbf{r}_k)}{|\mathbf{F}_l(\mathbf{r}_k)|} exp(-|e_k|) \qquad (2)$$

where e_k is the fixed charge located at $\mathbf{r}_k$ in the edge map. As $|e_k| \to 0$ in homogeneous areas, then $exp(-|e_k|) \to 1$, and the normalised Lorentz force $\mathbf{F}'_l(\mathbf{r}_k)$ has maximum magnitude tending to unity. When $|e_k|$ increases in edge

---

[1]*http://vision.cs.bris.ac.uk/AC/CCM/*   (includes larger versions of all images, as well as extended comparative results)

regions, $exp(-|e_k|)$ scales $\mathbf{F}'_l(\mathbf{r}_k)$ inversely proportional to the edge strength $|e_k|$ and so $\mathbf{F}'_l(\mathbf{r}_k)$ reaches its minimum at the strongest edge location. Thus, the normalised Lorentz force field has the strongest vector flows in homogeneous regions which start to attenuate smoothly when entering edge neighbourhoods. Fig. 2 shows an examples of an original and normalised Lorentz force field of a simple shape with both interior and exterior boundaries along with a close-up look into both fields. As can be seen the normalised field $\mathbf{F}'_l$ is much more functional than the original $\mathbf{F}_l$ field in homogeneous or edge regions in achieving the objective of speeding or steadying the contour respectively.
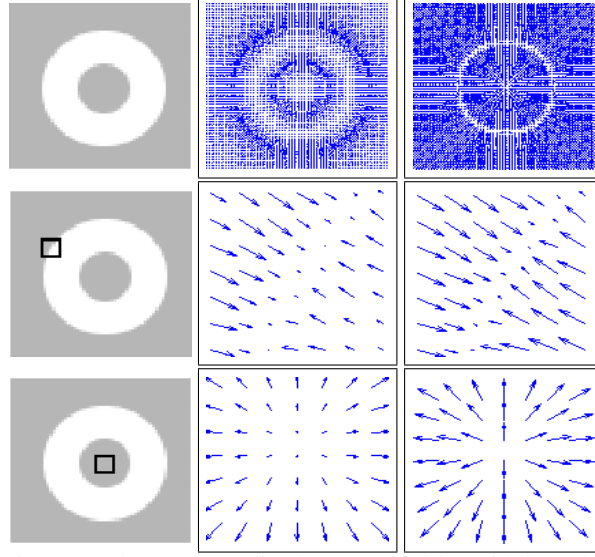
Figure 2. Top: Original image, its pre and post-normalised Lorentz fields, Middle and Bottom rows: close-ups on edge and homogeneous regions with pre and post-normalised fields respectively.

We then use curvature flow for contour regularisation based on [1] with our contour evolution function derived as:

$$\frac{\partial C}{\partial t} = \alpha g(x,y)\kappa\mathbf{N} + (1-\alpha)(\mathbf{F}'_l \cdot \mathbf{N})\mathbf{N} \tag{3}$$

where κ denotes the curvature flow, $g(x,y) = (1 + f(x,y))^{-1}$ is a stopping term, $\mathbf{N}$ denotes the contour inward normal, and α is a positive constant that balances the contribution from curvature flow regularisation and the Lorentz force attraction. The first term regulates the contour. The orientation of the Lorentz force field at a point is towards strong nearby edges and thus every point of the charged contour will be attracted towards these edges and stop there, whilst being maintained as a closed contour. We embed the charged contour in a level-set so that it can propagate in the normalised Lorentz force field with topological flexibility:

$$\frac{\partial u}{\partial t} = \alpha g(x,y)\kappa|\nabla u| - (1-\alpha)\mathbf{F}'_l \cdot \nabla u \tag{4}$$

where u denotes the level-set. As the geometric contour always propagates in the direction of its normal $\mathbf{N}$, it is unable to move when the Lorentz forces are tangent to the contour. We compensate for this by adding an extra adaptive balloon force similar to Paragios et al. [7]. Hence the final formulation of CCM becomes:

$$\frac{\partial C}{\partial t} = \alpha g(x,y)\kappa\mathbf{N} + (1-\alpha)\{(1-\gamma(\mathbf{F}'_l \cdot \mathbf{N}))(\mathbf{F}'_l \cdot \mathbf{N}) + \gamma(\mathbf{F}'_l \cdot \mathbf{N})g(x,y)sign(\mathbf{F}'_l \cdot \mathbf{N})\}\mathbf{N} \tag{5}$$

where $\gamma = exp(-\lambda|.|)$ is a zero-mean Laplacian function which balances the contributions from the Lorentz and extra balloon forces. When the Lorentz forces and the contour normal are close to orthogonal, the extra balloon force contributes to shrink or expand the contour based on $sign(\mathbf{F}'_l \cdot \mathbf{N})$. Otherwise, the contour propagates mainly under the influence of Lorentz forces. The final level set representation is:

$$\frac{\partial u}{\partial t} = \alpha g(x,y)\kappa|\nabla u| - (1-\alpha)\{(1-\gamma(F_N))(\mathbf{F}'_l \cdot \nabla u) + \gamma(F_N)g(x,y)sign(F_N)|\nabla u|\} \tag{6}$$

where $F_N = -\mathbf{F}'_l \cdot \frac{\nabla u}{|\nabla u|}$ is the component of $\mathbf{F}'_l$ along the contour inward normal $-\frac{\nabla u}{|\nabla u|}$. Fig. 3 shows the propagation of CCM on a synthetic image. Note, CCM does not need to be initialised completely exterior or interior to the objects. However, in practice, background noise and features dictate a more elaborate initialisation scheme (see next section).

Computation of the Lorentz force field based on (1) is a simple, yet intensive, method which leads to $O(M^2)$ complexity. Therefore, we use the Particle-Particle Particle-Mesh method, originally proposed in [3], for fast and accurate evaluation of Lorentz forces, as in the CPM model [4]. The reader is referred to [3] for details.
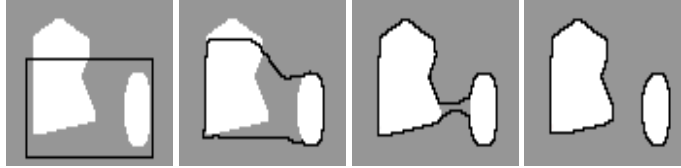
Figure 3. From left: the original image, initial CCM, and snapshots of contour propagation.

4 Automatic Initialisation

Here we propose a simple automatic initialisation method specifically designed for our cardiac SPECT application, although potentially it can be useful for other applications too. The divergence of a 2D vector field **F** is:

$$Div(\mathbf{F}) \equiv \nabla \cdot \mathbf{F} \equiv \frac{\partial F_x}{\partial x} + \frac{\partial F_y}{\partial y} \tag{7}$$

Therefore, the divergence values in a normalized image-based Lorentz force field, $Div(\mathbf{F}'_l)$, are usually negative in edge areas, and positive in homogeneous regions where the forces point at directions away from each other. We propose that if a point in the field where $Div(\mathbf{F}'_l(\mathbf{r}_k)) > 1$ is divergent enough to expand a contour, then it can be chosen as a candidate point for contour initialization. However, if we place an initial contour around every such candidate point, then contours propagating from both inside and outside an object will merge at the object boundaries due to the level-set formulation, and thus lead to false detection. Hence, we select the candidate points that are in the brightest regions of the image on the premise that these belong either to the object or the background. The contours then segment the object from *either the inside or the outside*. This works very well in practice for the cardiac SPECT images in which we used the top 20% of the brightest regions. This was determined empirically but is a very flexible threshold. Figure 4 shows an example of our automatic divergence point selection process, including a close-up of a divergence region and the entire divergence map.
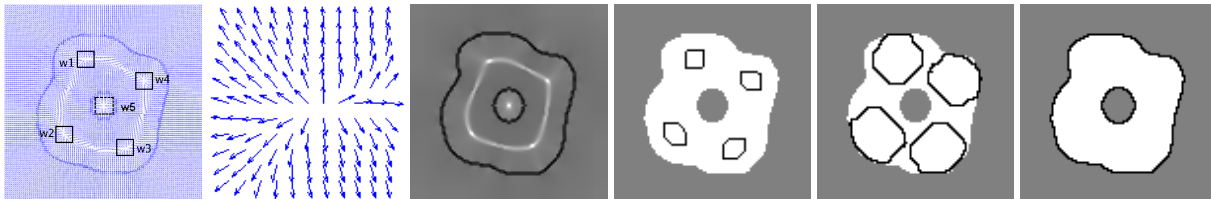
Figure 4. From left: Parts of the Lorentz force field where divergence is > 1 (i.e. w1-w5), close-up of w1, the divergence map with brightness proportional to divergence, automatic initialisation (w5 is discarded as it falls into the non-bright category), propagating CCM, final result.

5 Experiments

We applied our model to 64×64 pixel cardiac SPECT data of 20 individual patients, with 8 time frames per cardiac cycle. The parameters in the model were determined empirically and were kept constant throughout the experiments, i.e. $\lambda = 3$ and $\alpha = 0.1$. All patient studies were clinical studies acquired following standard protocols [8]. The results were evaluated against groundtruth data hand-labelled by an expert in SPECT imaging. Fig.5 shows snapshots of an evolving contour on an example LV image. Fig. 6 shows the initialisation and final contour results on a few more examples from our dataset, along with results from the CPM [4] model for comparison. The low resolution and largely diffused edges of the data impose a great burden on boundary detection, and CPM fails to recover most of the fuzzy edges (as described in Section 2) because particles inherently need to push along the boundaries. In comparison, CCM produces much better results as the contour propagates along its normal and can stabilise in the face of weaker edges.

We obtained 87.3% accuracy with $\sigma = 6.7\%$ in delineating the LV region across our dataset of 160 images based on a region overlap measure against the groundtruth data (itself subject to some human error). The best result was 98.8%, while the lowest was 60.7% where a large error resulted from extreme fuzziness of the edge areas due to the uptake of the radiotracer in the small bowel which can obscure the external border of the heart, particularly in the inferior wall.

6 Conclusions

We introduced a charged contour model for object detection based on charged particle dynamics and active contour propagation. An automatic initialisation method was also proposed to automate the model for convenient use in our
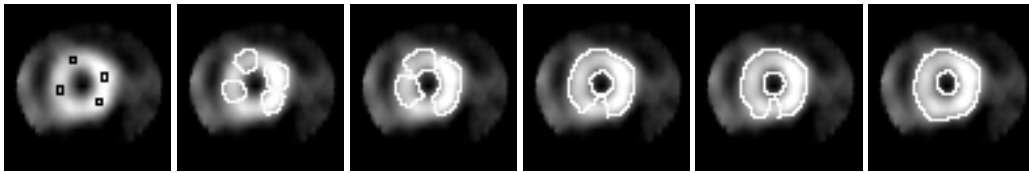
Figure 5. From left: Initial points of divergence, and snapshots of CCM detecting the internal and external boundaries of a LV on a short-axis cardiac SPECT.
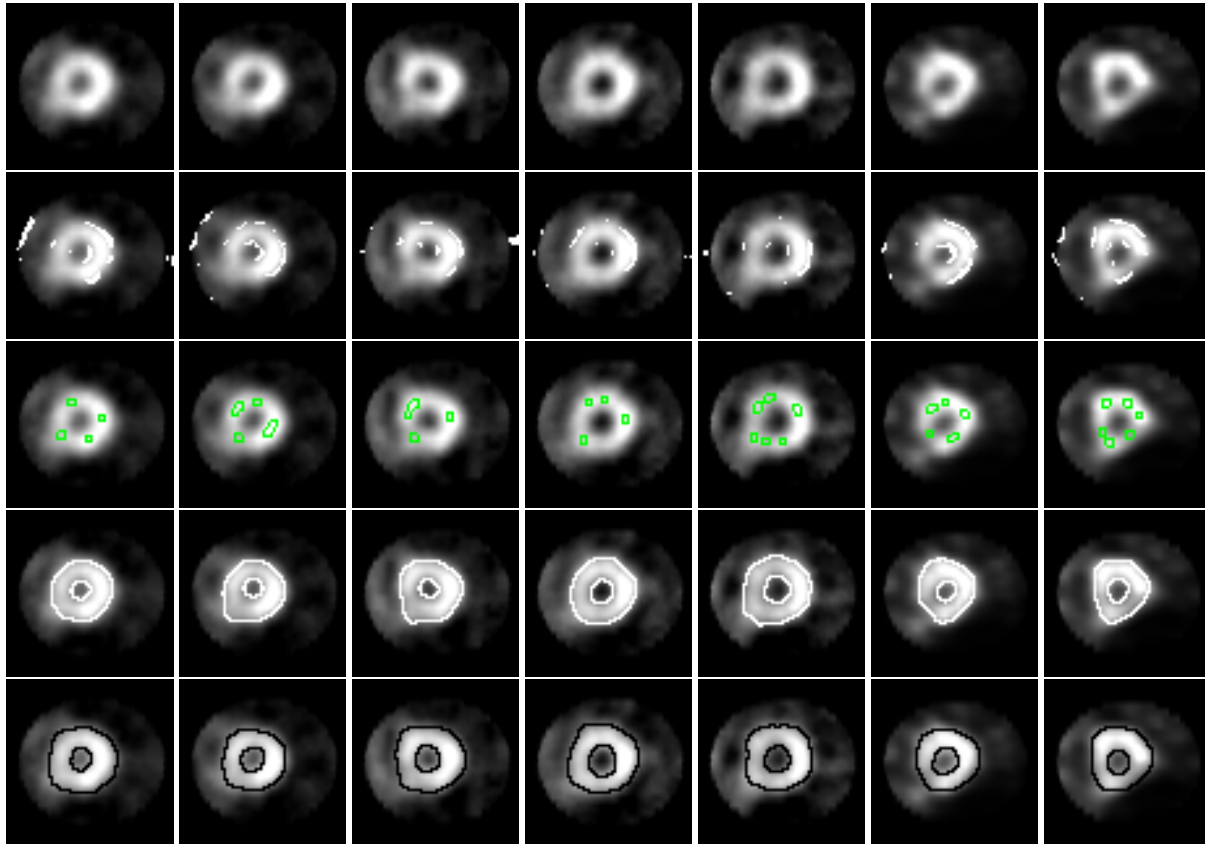
Figure 6. Mid-slice at 1st time frame from 7 different patients, from top to bottom: original image, CPM result, automatically initialized CCM, CCM result, and hand-labelled data.

cardiac SPECT application. A drawback of the current model is that it detects boundaries solely based on image gradients, and thus might lead to inaccurate definition of the internal and external borders of the LV, especially due to the fuzzy edges of SPECT data. Therefore, we aim to incorporate *a priori* knowledge constraints into the model such as constant myocardial volume for better LV segmentation and then motion estimation.

References

1. V. Caselles, R. Kimmel, and G. Sapiro. Geodesic active contours. In *ICCV*, pages 694–699, 1995.
2. E. Debreuve, M. Marlaud, G. Aubert, and J. Darcourt. Space time segmentation using level set active contours applied to myocardial gated SPECT. *IEEE Medical Imaging*, 20(7):643–659, 2001.
3. R.W. Hockney and J.W. Eastwood. *Computer Simulation Using Particles.* Taylor and Francis, 1988.
4. A.C. Jalba, M.H.F Wilkinson, and J.B.T.M Roerdink. CPM: A deformable model for shape recovery and segmentation based on charged particles. *IEEE PAMI*, 26(10):1320–1335, 2004.
5. P. Kass, A. Witkin, and D. Terzopoulos. Snakes: Active contour models. *IJCV*, 1:321–331, 1988.
6. R. Mullick and N. Ezquerra. Automatic segmentation of 3D cardiac SPECT imagery. In *IEEE SBEC*, pages 40–42, 1993.
7. N. Paragios, O. Mellina-Gottardo, and V. Ramesh. Gradient vector flow fast geodesic active contours. *IEEE PAMI*, 26(3):402–407, 2004.
8. T. Vakhtangandze, D.O. Hall, F.V. Zananiri, and M.R. Rees. The effect of Butterworth and Metz reconstruction filters on volume and ejection fraction calculation with ^{99}tc^{m} gated myocardial SPECT. *BJR*, 78:733–736, 2005.